

S1 Combustion conditions and primary emission

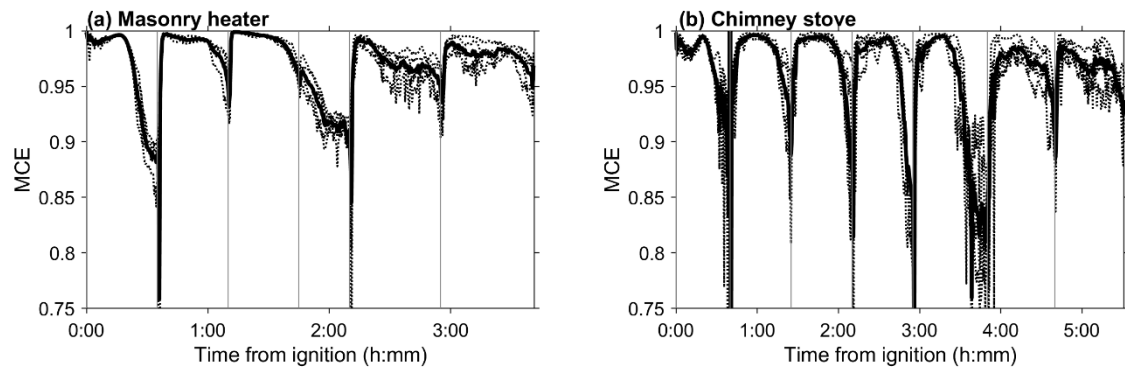


Figure S1: Modified combustion efficiency (MCE = $\Delta\text{CO}_2 / (\Delta\text{CO}_2 + \Delta\text{CO})$) during experiments. Averages over all experiments are shown with the solid lines and different experiments are shown with the dotted lines.

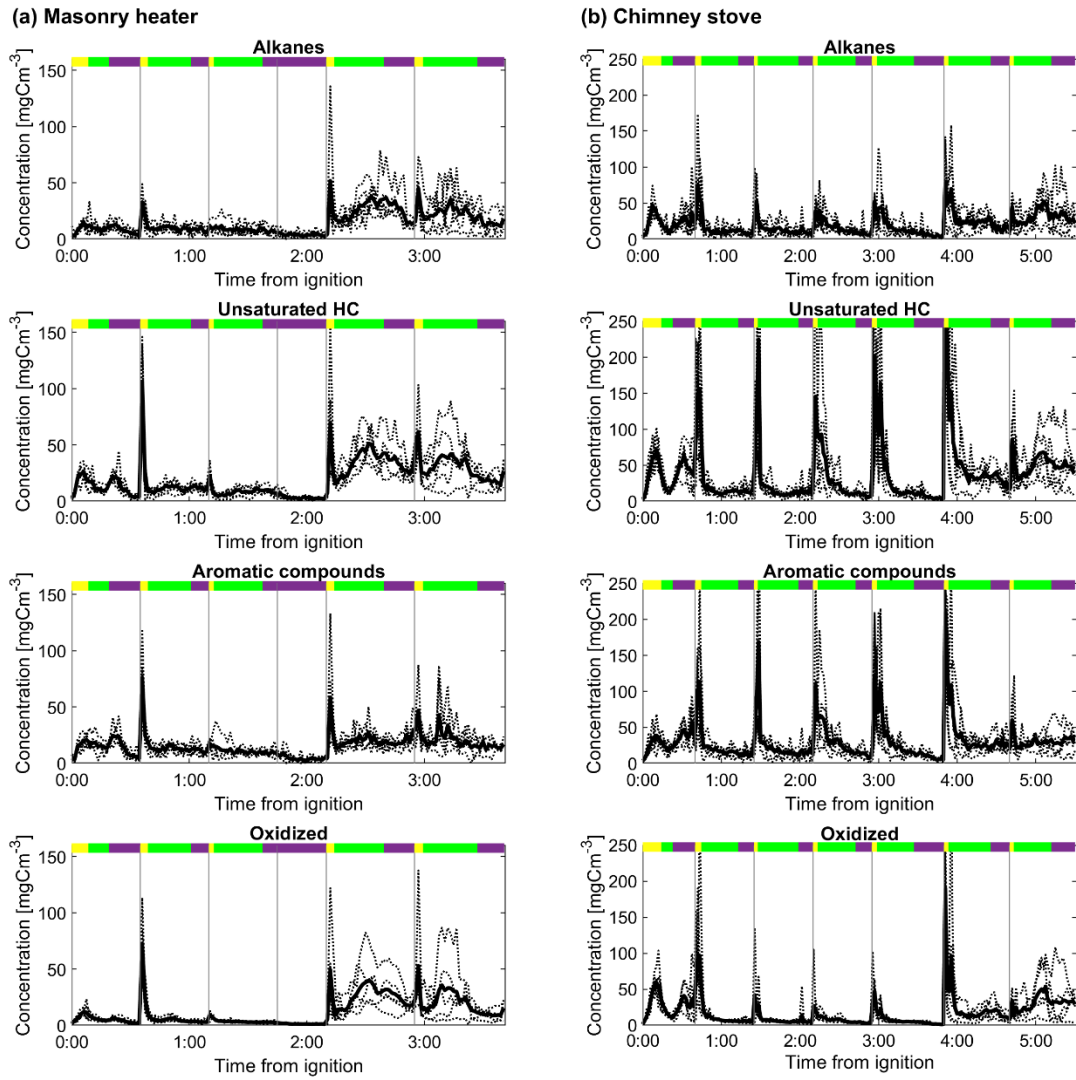
5 **Table S1: Compounds measured by FTIR and their reaction rates with OH (k_{OH})utilized for OHR_{ext} calculations.**

Compound	Formula	VOC group	CAS	Range	unit	k_{OH} [cm ³ /molec. s]
Water vapor	H ₂ O		7732-18-5	30	vol-%	2.10E-16
Carbon dioxide	CO ₂		124-38-9	25	vol-%	
Carbon monoxide	CO		630-08-0	5000	ppm	2.41E-13
				2	vol-%	
Nitrous oxide	N ₂ O		10024-97-2	200	ppm	2.01E-16
Nitrogen monoxide	NO		10102-43-9	1000	ppm	1.00E-11
Nitrogen dioxide	NO ₂		19192-44-0	200	ppm	1.06E-11
Sulfur dioxide	SO ₂		7446-09-5	1000	ppm	1.31E-12
Carbonyl sulfide	COS		483-58-1	100	ppm	1.96E-15
Ammonia	NH ₃		7664-41-7	500	ppm	1.57E-13
Hydrogen chloride	HCl		7647-01-0	200	ppm	7.86E-13
Hydrogen cyanide	HCN		74-90-8	100	ppm	3.13E-14
Hydrogen fluoride	HF		7664-39-3	100	ppm	
Methane	CH ₄		74-82-8	1000	ppm	6.28E-15
Ethane	C ₂ H ₆	Alkane	74-84-0	200	ppm	2.41E-13
Propane	C ₃ H ₈	Alkane	74-98-6	200	ppm	1.10E-12
Butane	C ₄ H ₁₀	Alkane	106-97-8	200	ppm	2.33E-12
Pentane	C ₅ H ₁₂	Alkane	109-66-0	200	ppm	3.80E-12
Hexane	C ₆ H ₁₄	Alkane	110-54-3	200	ppm	5.20E-12
Heptane	C ₇ H ₁₆	Alkane	142-82-5	200	ppm	6.76E-12
Octane	C ₈ H ₁₈	Alkane	111-65-9	200	ppm	7.43E-12
Acetylene	C ₂ H ₂	Unsaturated	75-86-2	200	ppm	7.75E-13
Ethylene	C ₂ H ₄	Unsaturated	74-85-1	200	ppm	8.51E-12
Propene	C ₃ H ₆	Unsaturated	115-07-1	200	ppm	3.01E-11
1,3-Butadiene	C ₄ H ₆	Unsaturated	106-99-0	200	ppm	6.93E-11
Benzene	C ₆ H ₆	Aromatic	71-43-2	200	ppm	1.28E-12
Toluene	C ₇ H ₈	Aromatic	108-88-3	200	ppm	6.16E-12
m-Xylene	C ₈ H ₁₀	Aromatic	108-38-3	200	ppm	2.45E-11
o-Xylene	C ₈ H ₁₀	Aromatic	95-47-6	200	ppm	1.47E-11
p-Xylene	C ₈ H ₁₀	Aromatic	106-42-3	200	ppm	1.52E-11
1,2,3-Trimethylbenzene	C ₉ H ₁₂	Aromatic	526-73-8	200	ppm	2.89E-11
1,2,4-Trimethylbenzene	C ₉ H ₁₂	Aromatic	95-63-6	200	ppm	3.16E-11
1,35-Trimethylbenzene	C ₉ H ₁₂	Aromatic	106-42-3	200	ppm	5.98E-11
Formic acid	CH ₂ O	Oxygenated	64-18-6	200	ppm	4.50E-13
Acetic acid	C ₂ H ₄ O ₂	Oxygenated	64-19-7	200	ppm	6.69E-13
Formaldehyde	CHOH	Oxygenated	50-0-0	200	ppm	9.38E-12
Acetaldehyde	C ₂ H ₄ O	Oxygenated	75-07-0	200	ppm	1.63E-11
Methanol	CH ₄ O	Oxygenated	67-56-1	500	ppm	9.28E-13
Ethanol	C ₂ H ₆ O	Oxygenated	64-17-5	500	ppm	3.24E-12
Propanol	C ₃ H ₈ O	Oxygenated	71-23-8	500	ppm	5.82E-12

Table S2: Average (\pm standard deviation) concentrations of gaseous emissions measured by FTIR for each experiment type (five experiments each).

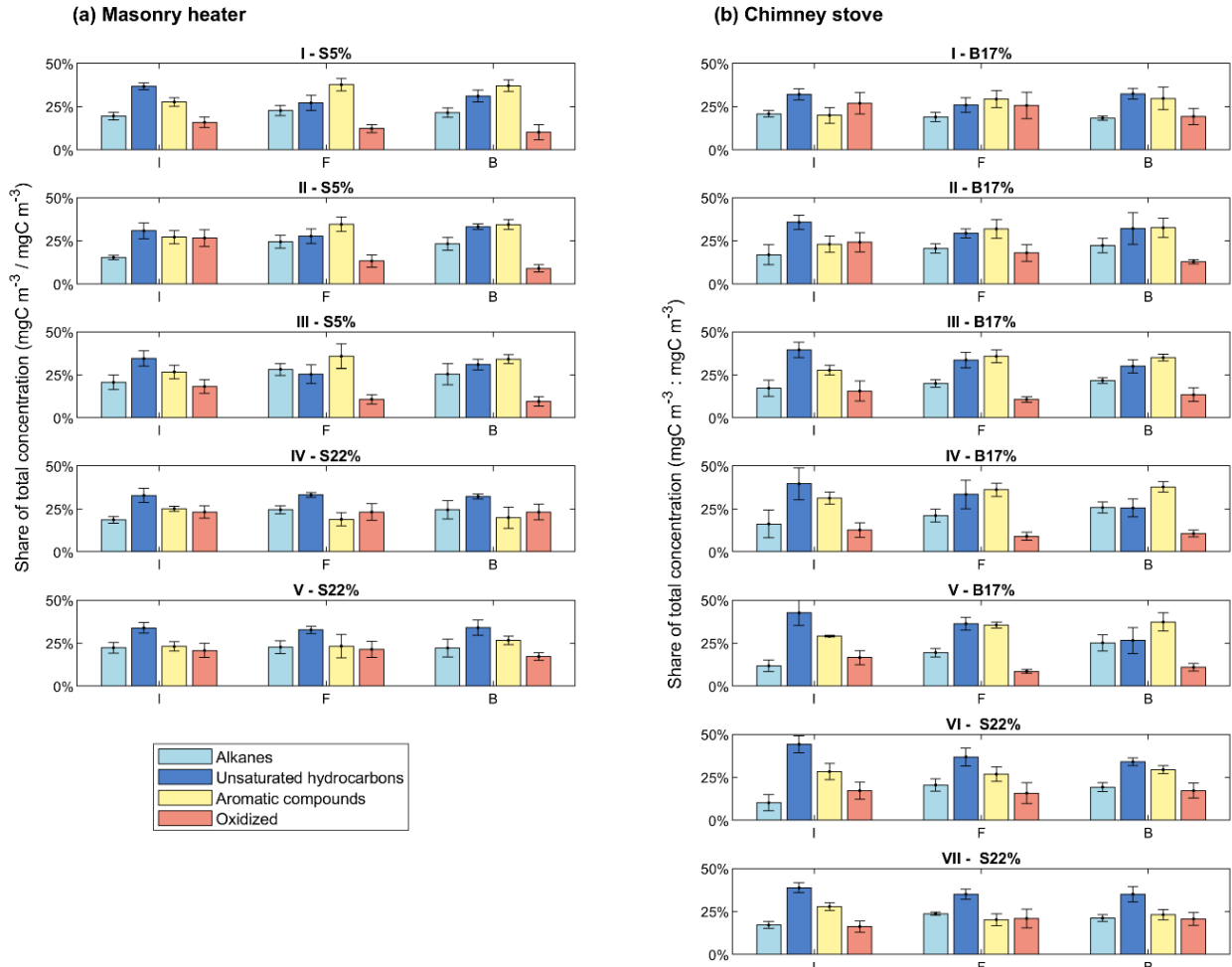
Compound	unit	Masonry heater		Chimney stove		Masonry heater; S-5% v. S-22%	Chimney stove; B-17% v. S-22%	S-22%; Masonry heater v. Chimney stove
		S-5%	S-22%	B-17%	S-22%			
Water vapor	vol-%	4.5 \pm 0.3	4.1 \pm 0.4	7.2 \pm 0.4	6.4 \pm 0.5	<0.01	<0.01	<0.01
Carbon dioxide	vol-%	4.6 \pm 0.1	3.26 \pm 0.08	6.2 \pm 0.3	5.9 \pm 0.4	<0.01	0.05	<0.01
Carbon monoxide	ppm	638 \pm 26.5	735 \pm 129	1680 \pm 249	1880 \pm 144	0.24	0.28	<0.01
Nitrogen monoxide	ppm	25.6 \pm 1.8	21.4 \pm 2.6	45.9 \pm 2.9	31.6 \pm 3.7	<0.01	<0.01	<0.01
Nitrogen dioxide	ppm	1.0 \pm 0.4	2.7 \pm 1.1	1.3 \pm 0.7	2.6 \pm 1.6	0.03	0.08	0.98
Sulfur dioxide	ppm	0.5 \pm 0.3	0.6 \pm 0.3	1.4 \pm 0.3	0.9 \pm 0.1	0.05	<0.01	0.1
Ammonia	ppm	1 \pm 0.3	1.9 \pm 0.3	6.2 \pm 0.4	5.1 \pm 0.5	<0.01	0.01	<0.01
Methane	mgC m ⁻³	10.5 \pm 0.5	23.6 \pm 5.6	28.7 \pm 4.5	46.3 \pm 4.4	<0.01	0.01	<0.01
Non-methane VOCs	mgC m ⁻³	42.6 \pm 9.2	101 \pm 24.6	89.4 \pm 11.3	148.3 \pm 23	0.01	<0.01	0.05
Alkanes	mgC m ⁻³	9.7 \pm 2.6	23.8 \pm 6.6	16.9 \pm 3	29.5 \pm 6.7	<0.01	0.01	0.31
Unsaturated	mgC m ⁻³	12.8 \pm 2.9	33.1 \pm 8.1	30.8 \pm 4.7	54.2 \pm 5.4	<0.01	<0.01	<0.01
Aromatics	mgC m ⁻³	14.2 \pm 3.5	20.7 \pm 2.6	27.9 \pm 4.9	36.0 \pm 3.4	0.02	0.02	<0.01
Oxygenated	mgC m ⁻³	5.6 \pm 1.2	21.9 \pm 8.1	13.3 \pm 0.6	27.1 \pm 8.9	0.01	0.04	0.51

* paired Student's t-test; comparison of averages of the consecutive experiments; ** unpaired Student's t-test of independent experiments



10

Figure S2: Timeseries of VOC emissions from (a) masonry heater and (b) chimney stove for the four VOC groups. Average lengths of the combustion phases are marked on the top panel with the yellow (ignition), green (flaming), and purple (burnout).



15 **Figure S3: Average shares of the VOC groups at different combustion phases (I = ignition, F = flaming, B = burnout) for each batch (I-V for masonry heater, I-VII for chimney stove) as a relation to the total VOC concentration (mgC m⁻³ / mgC m⁻³) measured by FTIR from the fresh exhaust. Error bars denote standard deviations.**

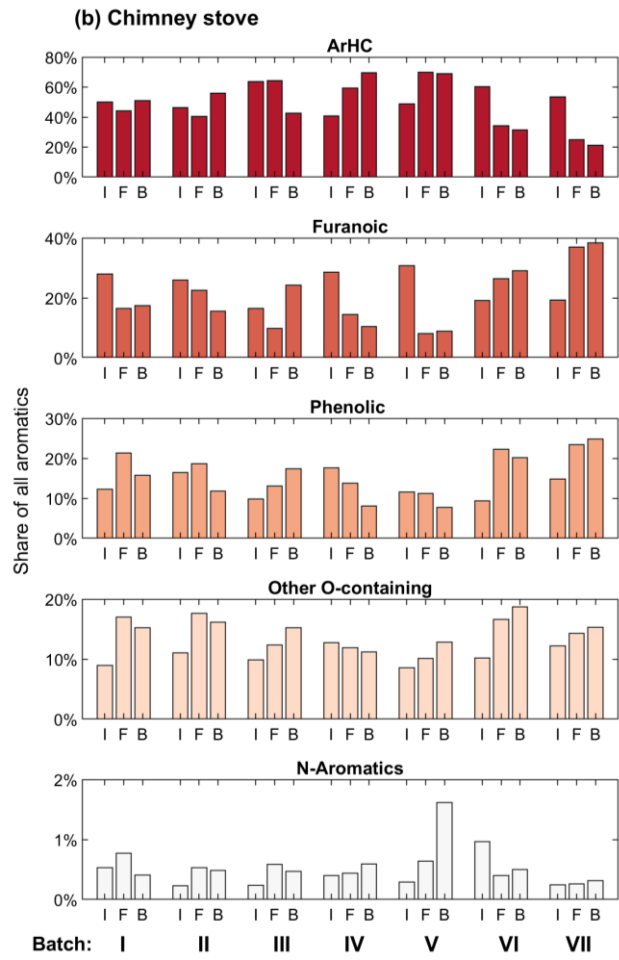
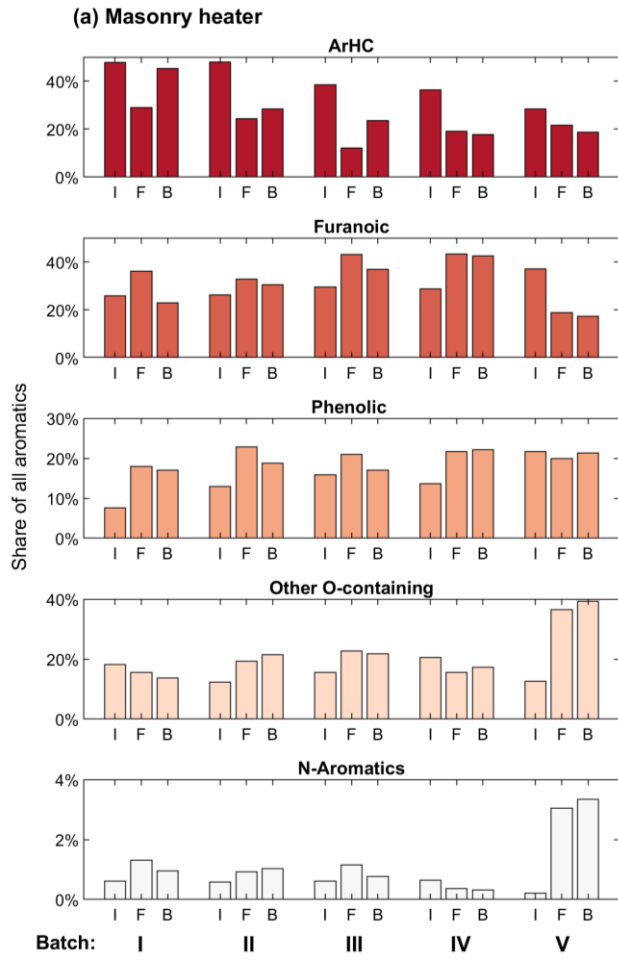


Figure S4: Shares of aromatic compound groups measured by the PTR-ToF-MS from unaged aerosol, in relation to the total aromatic concentration (ppm/ppm) during different combustion phases (I = ignition, F = flaming, B = burnout) for each batch.

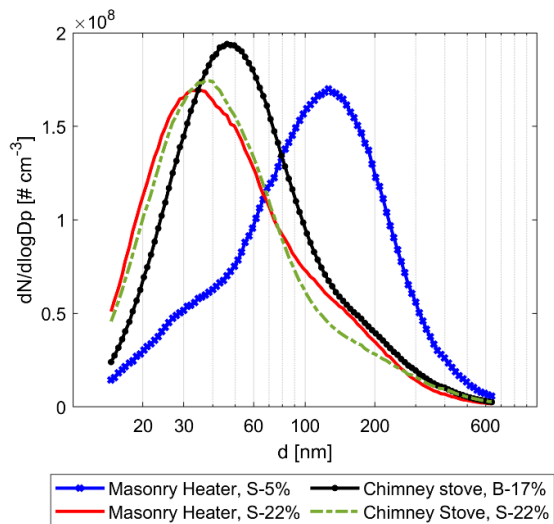


Figure S5: Average size distributions in the primary exhaust (dry, 13 % O₂) measured by SMPS.

S2 Conditions in PEAR

25 S2.1 External OH reactivity

External OH reactivity ($OHR_{ext} = \sum k_i \cdot c_i$) was calculated from the compounds measured by FTIR from the primary exhaust, using their reaction rate constants with OH (k_i ; Table S1) and dilution corrected concentrations (c_i) in the PEAR.

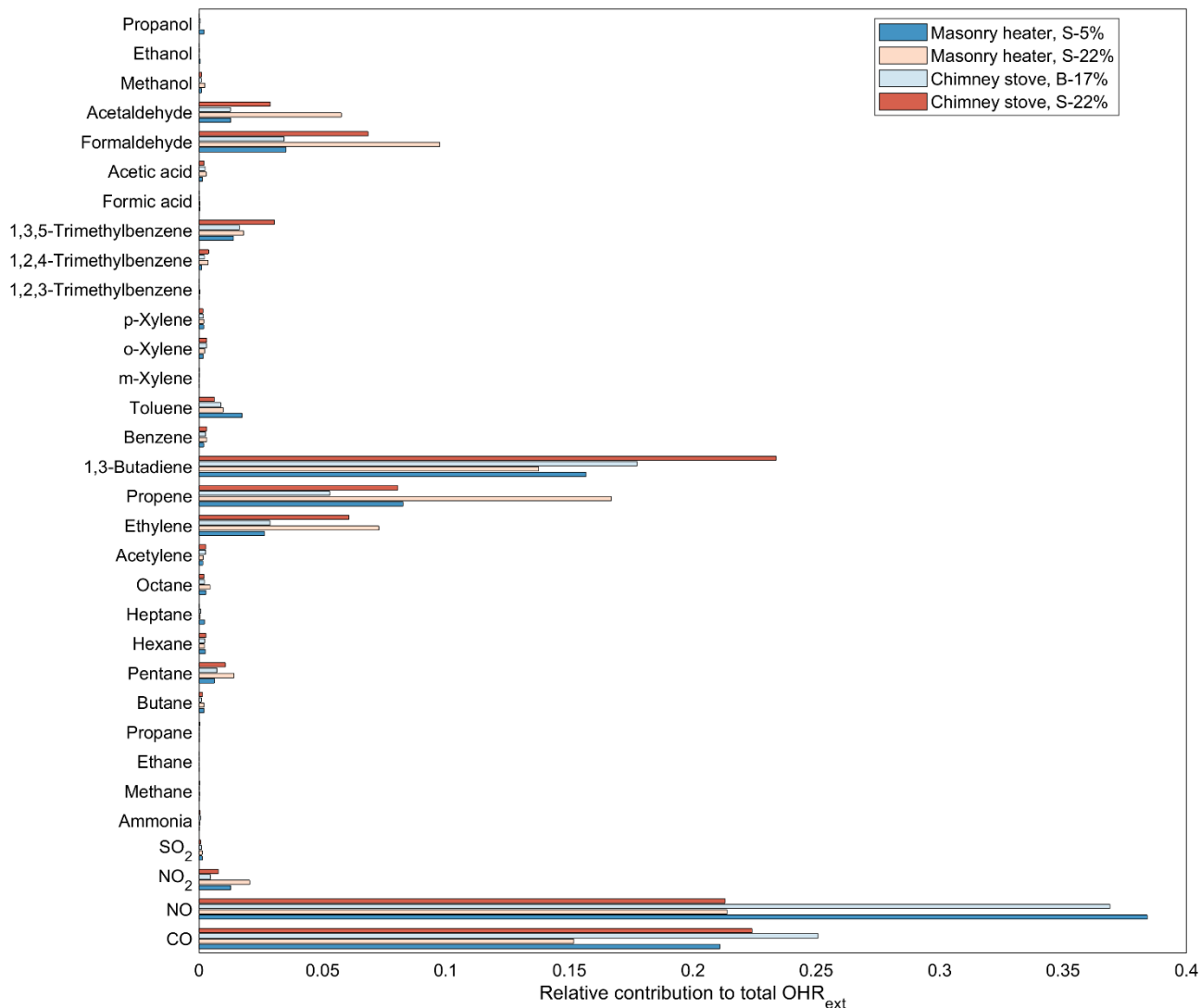
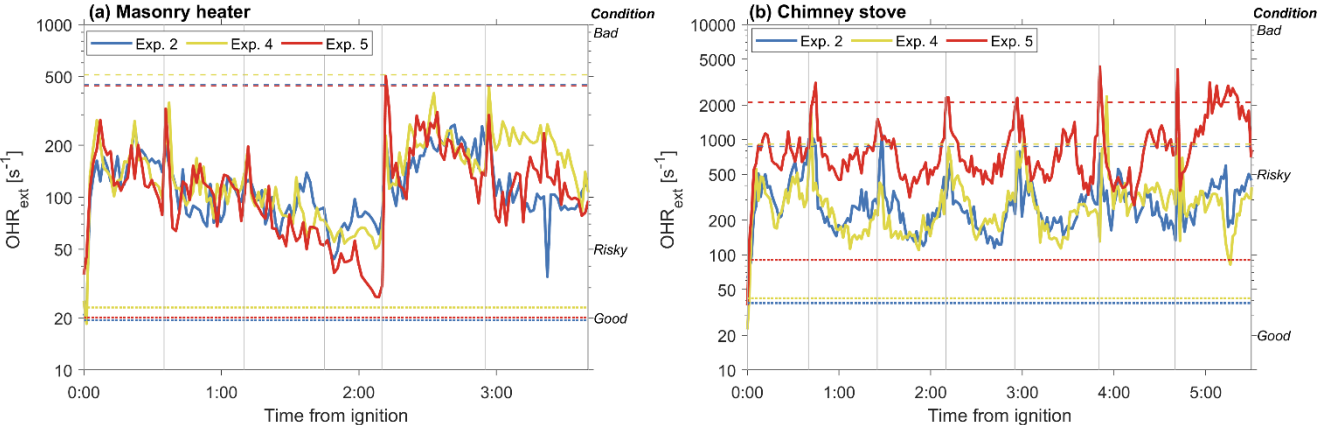


Figure S6: Average relative contributions of the measured gaseous compounds to the total OHR_{ext}.



30

Figure S7: External OH reactivity in the PEAR for the compounds measured by FTIR during photochemical aging experiments. Risk levels for OHR_{ext} , determined by Peng and Jimenez (2017), are marked with dotted (good/risky: $\frac{\text{Flux}_{254\text{nm}} \text{ exposure}}{\text{OH exposure}} > 4E5 \text{ cm s}^{-1}$) and dashed (risky/bad: $\frac{\text{Flux}_{254\text{nm}} \text{ exposure}}{\text{OH exposure}} > 1E7 \text{ cm s}^{-1}$) lines for each experiment.

S2.2 Fate of low-volatility organic compounds in the PEAR

Estimations of the LVOC fates in the PEAR were done based on Palm et al. (2016). Three possible pathways for LVOC depletion in the PEAR were considered: condensation onto particles, reactions with OH, and condensation onto walls of the PEAR. The rest exit the PEAR in the gas-phase after which they are expected to condense on the walls of sampling lines.

The LVOC lifetime due to aerosol losses (τ_{aer}) was calculated using Eq. (S1):

$$\tau_{\text{aer}} = \frac{1}{\text{CS}} \quad (\text{S1})$$

where condensation sink (CS, s^{-1} ; Fig 4) was calculated according to Lehtinen et al. (2003), using an average of the particle size distributions before and after the PEAR. The diffusion coefficient in use (D ; $7 \times 10^{-6} \text{ m}^2 \text{ s}^{-1}$) was chosen as representative for oxidised, $\sim 200 \text{ g mol}^{-1}$ molecules (Tang et al., 2015).

LVOC lifetime due to wall losses (τ_{wall}) was calculated with Eq. (S2):

$$\tau_{\text{wall}} = \left(\frac{A}{V} * \frac{2}{\pi} \sqrt{k_e D} \right)^{-1} \quad (\text{S2})$$

τ_{wall} depends on the area-to-wall ratio ($\frac{A}{V}$), which in the PEAR is $2.28 \text{ m}^2 : 0.139 \text{ m}^3 = 16.4 \text{ m}^{-1}$. The applied eddy diffusion coefficient, k_e , was 0.0036 s^{-1} , similarly to Palm et al. (2016). τ_{wall} was constant (603 s) for all of the PEAR experiments.

Lifetime for LVOCs due to reactions with OH radicals was calculated with Eq. (S3):

$$\tau_{\text{OH}} = \frac{5}{k_{\text{OH}*} [\text{OH}]} \quad (\text{S3})$$

based on the estimations that LVOCs as a total have an OH reaction rate (k_{OH}) of $1 \times 10^{-11} \text{ cm}^3 \text{ molec.}^{-1} \text{ s}^{-1}$ and that it takes five such reactions for LVOC fragmentation into higher-volatility compounds.

The resulting total lifetime was calculated with Eq. (S4):

$$\tau_{total} = \left(\frac{1}{\tau_{aer}} + \frac{1}{\tau_{wall}} + \frac{1}{\tau_{OH}} \right)^{-1} \quad (S4)$$

from which the fraction of each pathway (F_x , where footnote denotes the degradation pathway: aerosol, wall, or OH) to the total loss was derived with eq. (S5).

55

$$F_x = (1 - F_{exit}) * \frac{\tau_x^{-1}}{\tau_{total}^{-1}} \quad (S5)$$

The fraction of LVOCs exiting the PEAR in gas-phase (F_{exit}) was by eq. (S6):

$$F_{exit} = e^{-\frac{RT}{\tau_{total}^{-1}}} \quad (S6)$$

with the residence time (RT) being 139s for the 60lpm flow rate.

S2.3 Photochemical exposure in PEAR

60 OH exposure during photochemical aging was measured directly from the decay of added butanol-*d*9, similarly to Barmet et al. (2012). Timeseries for the OH exposures during each experiment are shown in Figure S8.

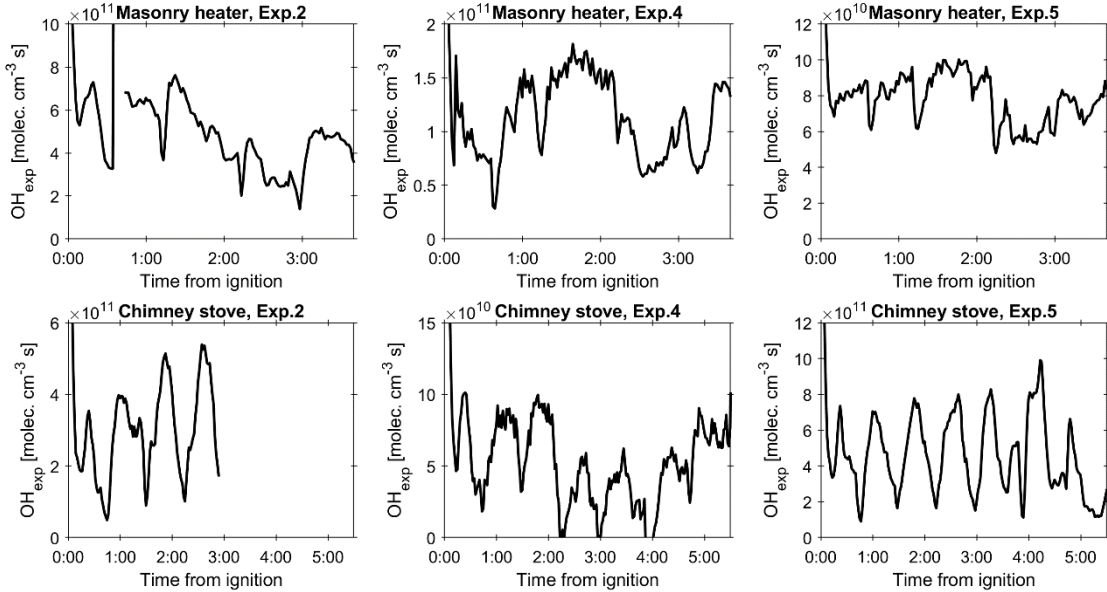


Figure 8: OH exposure during photochemical aging experiments.

The relevance of other reaction pathways in the PEAR, including photolysis as well as exposure to ozone, excited singlet 65 oxygen ($O(^1D)$), and triplet atomic oxygen ($O(^3P)$), was estimated based on the estimation equations by Peng et al. (2016) (Table S3). The conditions in the PEAR were assessed utilising the directly measured OH exposure (OH_{exp}), initial O_3 input concentration ($O_3,_{init}$), residence time in PEAR (RT; 139s), and water mixing ratio (H_2O ; 0.015 for 45 % relative humidity). Average exposures during each experiment are shown in Table S4, and their relevance towards ambient atmospheric conditions are displayed in Figure S11.

Table S3: Estimation equations used for determination of photon flux ($F_{254\text{nm}}$), O(³P), O(¹D), and O₃ exposures, based on Peng et al. (2016).

Reactant	Exposure estimation equation	eq.no
Photon flux	$flux_{254\text{nm},exp} = 10^{(1.0238 + \sqrt{(-1.0238)^2 - 4 * 0.060786 * c}) / 2 * 0.060786}$ $\text{where } c = - \left[\log_{10} \left(OH_{exp} * \frac{180}{RT} \right) - \left\{ 15.514 + 0.79292 * \log_{10}(H_2O) + 0.023076 * \log_{10}(H_2O)^2 - \log_{10} \left(1 + e^{\frac{-0.42602 - \log_{10}(\frac{O_{3,init}}{OHR_{ext}})}{0.39479}} \right) \right\} \right]$	(S7)
O(¹ D)	$\log_{10}(O(^1D)_{exp}) = 3.7371 + 0.1608 * \log_{10} \left(-\log_{10} d^{\frac{180}{RT}} \right)$ $- 1.1344 * \log_{10} H_2O + 0.59179 * \log_{10} O_{3,init}$ $- 0.17019 * \log_{10} \left(-\log_{10} d^{\frac{180}{RT}} \right) * \log_{10} H_2O$ $- 0.37983 * \log_{10} \left(-\log_{10} d^{\frac{180}{RT}} \right)^2 + 0.099941 * \log_{10} OHR_{ext}$	(S8)
O(³ P)	$\log_{10}(O(^3P)_{exp}) = 7.6621 + 0.16135 * \log_{10} \left(-\log_{10} d^{\frac{180}{RT}} \right)$ $- 1.1342 * \log_{10} H_2O + 0.59182 * \log_{10} O_{3,init}$ $- 0.17007 * \log_{10} \left(-\log_{10} d^{\frac{180}{RT}} \right) * \log_{10} H_2O$ $- 0.3797 * (\log_{10} \left(-\log_{10} d^{\frac{180}{RT}} \right))^2 + 0.099902 * \log_{10} (OHR_{ext})$	(S9)
O ₃	$\log_{10}(O_{3,exp}) = 15.559 + \log_{10} O_{3,init} + 0.42073 * \log_e(d^{180/RT})$	(S10)
for eq. S8-S10:	$d = \left(10^{-10}^{\log_{10}(OH_{exp}/RT*180) - 13.322 + 0.22101 * \left(\frac{OHR_{ext}}{O_{3,init}} \right)^{0.43529}} \right)^{RT/180}$	(S11)

75 **Table S4: Average exposures to radicals in the PEAR during photochemical aging experiments.**

	O ₃ input	photon flux		OH _{exp}	O(¹ D) _{exp}	O(³ P) _{exp}	O ₃ exp
	Exp.	[ppm]	[photons cm ⁻²]	Fuel	[# s cm ⁻³]	[# s cm ⁻³]	[# s cm ⁻³]
Masonry heater	2	2.3	8.3E+15	S-5%	5.8E+11	1.28E+6	1.07E+10
				S-22%	3.5E+11	1.16E+6	9.75E+9
	4	2.2	1.9E+15	S-5%	8.1E+10	3.74E+5	3.14E+9
				S-22%	6.3E+10	6.25E+5	5.25E+9
Chimney stove	5	1.8	1.36E+15	S-5%	8.1E+10	2.88E+5	2.42E+9
				S-22%	6.3E+10	3.83E+5	3.22E+9
	2	4.3	5.42E+15	B-17%	3.1E+11	1.51E+6	1.27E+10
				S-22%*	not meas.	not meas.	not meas.
	4	3.6	1.09E+15	B-17%	5.4E+10	3.08E+5	2.59E+09
				S-22%	6.1E+10	4.10E+5	3.45E+09
	5	11	1.06E+16	B-17%	5.0E+11	4.22E+6	3.55E+10
				S-22%	5.0E+11	5.04E+6	4.24E+10

* Direct OH exposure measurements not available for Chimney stove Exp. 2 S-22%; approximately similar as in Exp.2 B-17%.

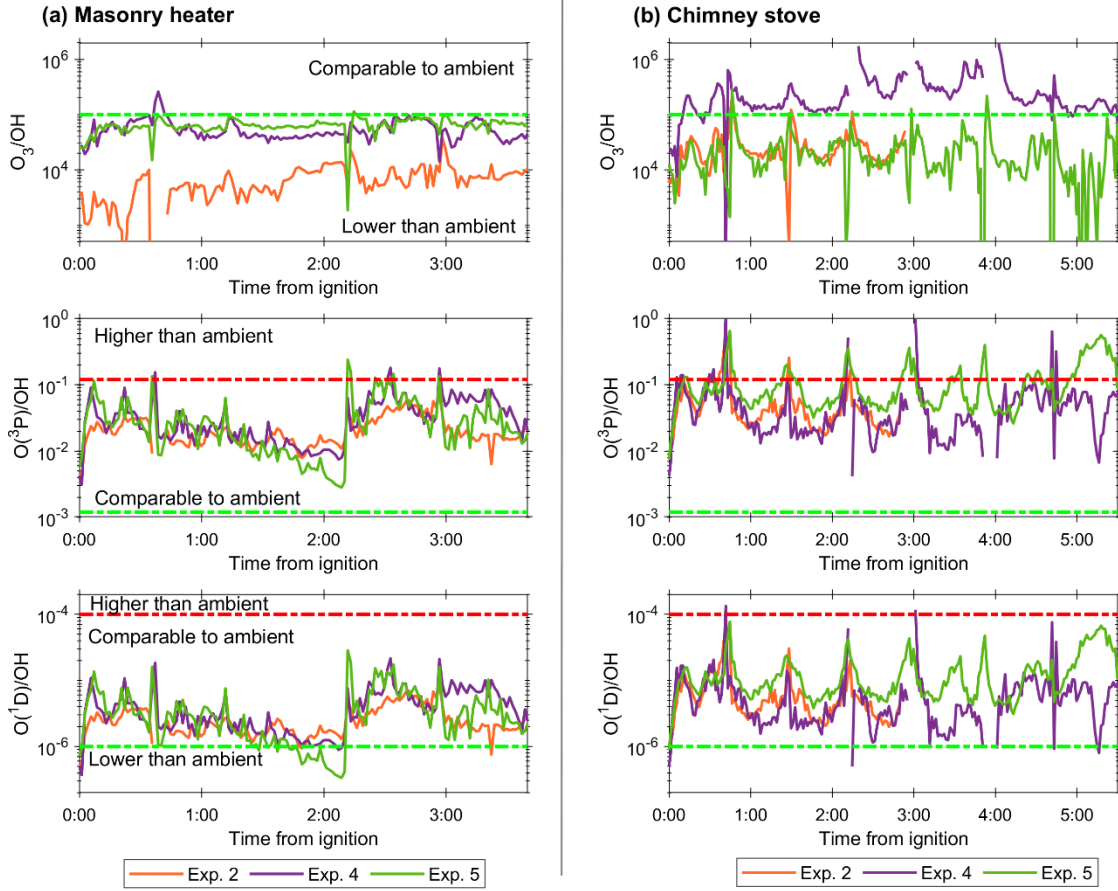


Figure S9: Ratios of alternative reaction pathways to the OH exposure. Ambient ratios as in Peng et al. (2016)

- 80 As an example of the relevance of the different reaction pathways, their importance towards the VOC fates was assessed for two important SOA precursors common for RWC: benzene and toluene (Fig. S10). The ratio of degradation by photolysis (D_{flux}) and reactions with alternative oxidants (D_x) to the degradation by OH reactions were calculated with Eq. (S12-S13), which show the inverse relationship between the importance of the pathway and the ratio of the photoabsorption cross section (σ_{abs}) or reaction rate of the compound with the considered radical ($k[X]_{VOC}$) to its reaction rate with OH ($k[OH]_{VOC}$).

$$D_{flux} = \frac{flux_{exp}}{[OH]_{exp}} * \frac{\sigma_{abs,VOC}}{k[OH]_{VOC}} \quad (S12)$$

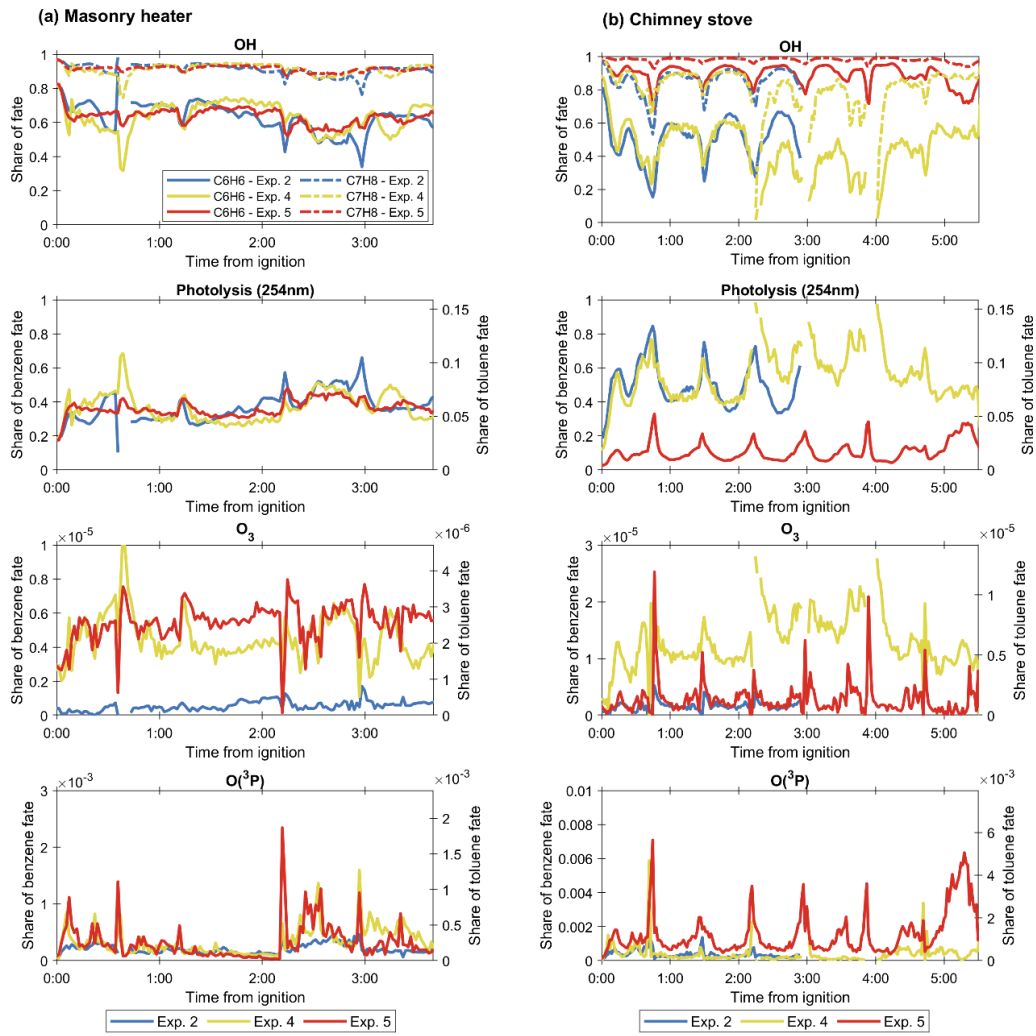
$$D_x = \frac{[X]_{exp}}{[OH]_{exp}} * \frac{k[X]_{VOC}}{k[OH]_{VOC}} \quad (S13)$$

The absorption cross sections and reactivities used for the exemplary pathway estimations for toluene and benzene are listed
90 in Table S5. The total degradation in relation to degradation by OH was calculated with eq. (S14) by considering reactions
with OH, O₃, and O(³P) and photolysis.

$$D_{total} = 1 + D_{flux} + D_{O_3} + D_{O(3P)} \quad (S14)$$

Table S5: Absorption cross sections (σ_{abs} , $\text{cm}^2 \text{molecule}^{-1}$) and reaction rates [$\text{cm}^3 \text{molec.}^{-1} \text{s}$] of major RWC VOCs towards oxidants in PEAR

	Benzene	Toluene	Phenol	Furan	Acetic acid	Acetaldehyde	Isoprene	References
$\sigma_{abs, 254\text{nm}}$	3.0E-19	2.3E-19	1.6E-18	7.1E-19*	4.8E-21	1.5e-20	5.3E-20	Keller-Rudek et al. (2015); * at 225nm
k[OH]	1.8E-12 ^A	6.16E-12 ^A	1.00E-11 ^B	4.04E-11 ^A	8.00E-13 ^C	1.62E-11 ^A	1.00E-10 ^A	A: (Atkinson, 1986), B: (Baulch et al., 1992); C: (Atkinson. et al., 2001)
k[O ₃]	1.72E-22 ^A	3.90E-22 ^A		2.42E-18 ^B		3.40E-20 ^c	1.29E-17 ^D	A: (Toby et al., 1985), B: (Atkinson et al., 1983) C: (Stedman and Niki, 1973), D: (Grosjean and Grosjean, 1996)
k[O(³ P)]	1.99E-14 ^A	7.63E-14 ^A	1.56E-13 ^B		1.73E-15 ^C	4.58E-13 ^B	3.50E-11	A: (Cvetanović, 1987), B: (Baulch et al., 1994), C: (Herron, 1988), (Paulson et al., 1995)



95

Figure S10: Share of the considered pathways in the total degradation of benzene and toluene in the PEAR during the experiments.

S3 Secondary gaseous phase

100

Table S6: Compounds identified from the RWC exhaust by PTR-ToF-MS and the applied reaction rates with H₃O⁺ (Cappellin et al., 2012).

Group	m/z	Ion	Suggested compound	k-rate	Group	m/z	Ion	Suggested compound	k-rate
Aliphatic hydrocarbons									
	53.04	C4H4-H ⁺	Butyne	2.00		45.03	C2H4O-H ⁺	Acetaldehyde	3.07
	55.06	C4H6-H ⁺	1,3-Butadiene	1.80		55.02	C3H2O-H ⁺	2-propynal	2.00
	67.06	C5H6-H ⁺	1,3-cyclopentadiene	1.83		57.03	C3H4O-H ⁺	Acrolein	3.49
	69.07	C5H8-H ⁺	Isoprene	1.95		71.02	C3H2O2-H ⁺	Propiolic acid	2.00
	97.11	C7H12-H ⁺	Cycloheptene	2.00		71.05	C4H6O-H ⁺	Methyl vinyl ketone, methacrolein	3.20
	109.10	C8H12-H ⁺	e.g. Cyclohexene, 4-ethenyl-	2.00		73.03	C3H4O2-H ⁺	2-Propenoic acid	2.60
	137.13	C10H16-H ⁺	Monoterpenes	2.42		75.04	C3H6O2-H ⁺	Hydroxy-2-propanone	2.33
						83.01	C4H2O2-H ⁺	3-Cyclobutene-1,2-dione	2.00
Aromatic hydrocarbons									
	79.05	C6H6-H ⁺	Benzene	1.93		85.07	C5H8O-H ⁺	e.g. Pentenal	2.00
	93.07	C7H8-H ⁺	Toluene	2.08		87.05	C4H6O2-H ⁺	e.g. 2,3- butadiene	1.70
	105.07	C8H8-H ⁺	Styrene	2.27		99.08	C6H10O-H ⁺	e.g. Hexenal	3.74
	107.09	C8H10-H ⁺	Xylene, ethylbenzenes	2.26		101.06	C5H8O2-H ⁺	e.g. Acetylacetone	2.93
	119.08	C9H10-H ⁺	e.g. Indane, methylstyrene	2.00		103.04	C4H6O3-H ⁺	Acetic anhydride	2.00
	121.10	C9H12-H ⁺	C3 benzene; e.g. Cumene	2.40		103.08	C5H10O2-H ⁺	e.g. Methyl-butyric acid	2.00
	129.07	C10H8-H ⁺	Naphthalene	2.45		117.02	C4H4O4-H ⁺	Fumaric acid	2.00
	143.09	C11H10-H ⁺	Methylnaphthalene	2.71		117.06	C5H8O3-H ⁺	e.g. Acetoxypipronone	2.00
	155.08	C12H10-H ⁺	e.g. Acenaphthene	2.82					
	167.08	C13H10-H ⁺	Fluorene	2.88					
Phenolic compounds									
	95.05	C6H6O2-H ⁺	Phenol	2.20		59.05	C3H6O-H ⁺	Acetone, propanal	3.20
	109.07	C7H8O-H ⁺	Cresols	3.20		61.03	C2H4O2-H ⁺	Acetic acid, glycolaldehyde	2.30
	111.04	C6H6O2-H ⁺	Benzenediols	2.00		73.07	C4H8O-H ⁺	2-butanone and 2-methylpropanal	3.12
	123.08	C8H10O-H ⁺	Dimethylphenol	2.00		77.02	C2H4O3-H ⁺	Acetic acid, hydroxy-	2.00
	125.06	C7H8O2-H ⁺	Guaiacol	2.00		89.03	C3H4O3-H ⁺	E.g. Acetic acid anhydride with formic acid	2.00
	139.04	C7H6O3-H ⁺	e.g. Salicylic acid	2.00		89.06	C4H8O2-H ⁺	Acetoin	4.23
	139.08	C8H10O2-H ⁺	Creosol, Trosol	2.00		99.01	C4H2O3-H ⁺	Maleic anhydride	2.00
	153.07	C8H8O3-H ⁺	e.g. Methoxy-benzoic acid	2.00		101.02	C4H4O3-H ⁺	Succinic anhydride	2.00
						105.04	C4H8O3-H ⁺	e.g. Acetic acid, methoxy-	2.00
Furanoic compounds									
	69.03	C4H4O-H ⁺	Furan	1.70		47.05	C2H6O-H ⁺	Ethanol	2.11
	83.05	C5H6O-H ⁺	Methylfuran	2.00		49.03	CH4O2-H ⁺	Methyl peroxide or methanediol	2.00
	85.03	C4H4O2-H ⁺	Furanone	2.00		63.04	C2H6O2-H ⁺	ethanediol	1.47
	97.03	C5H4O2-H ⁺	Furfural	3.95		77.05	C3H8O2-H ⁺	e.g. Ethanol 2-methoxy- ; 1,3-Propanediol	3.50
	97.07	C6H8O-H ⁺	Dimethyl- & ethyl furan	2.00		81.04	C5H4O-H ⁺	2,4-Cyclopentadiene-1-one	2.00
	99.04	C5H6O2-H ⁺	Furfuryl alcohol	2.00		91.07	C4H10O2-H ⁺	Butanediols	2.00
	119.05	C8H6O-H ⁺	Benzofuran	2.00		111.08	C7H10O-H ⁺	e.g. Heptenedial or trimethylfuran	2.00
	125.02	C6H4O3-H ⁺	2,5-Furandicarboxaldehyde	2.00		113.02	C5H4O3-H ⁺	e.g. 2-furoic acid	2.00
	127.04	C6H6O3-H ⁺	5-Hydroxymethylfurfural	2.00		113.06	C6H8O2-H ⁺	e.g. Methylcyclohexanone	2.00
						115.04	C5H6O3-H ⁺	e.g. Hydroxymethylfuranone	2.00
Nitroaromatics									
	140.03	C6H5NO3-H ⁺	Nitrophenols	2.00		115.08	C7H10O2-H ⁺		2.00
	154.06	C7H7NO3-H ⁺	e.g. Nitrocresol	2.00		115.11	C7H14O-H ⁺	e.g. Heptanal	2.83
Other oxygenated aromatics									
	107.05	C7H6O-H ⁺	Benzaldehyde	3.73		117.09	C6H12O2-H ⁺		2.00
	109.03	C6H4O2-H ⁺	Benzquinones	1.99		127.08	C7H10O2-H ⁺		2.00
	121.07	C8H8O-H ⁺	E.g. Acetophenone	3.36		139.11	C9H14O-H ⁺		2.00
	123.04	C7H6O2-H ⁺	Benzic acid	2.68		145.05	C6H8O4-H ⁺	e.g. Dimethyl fumarate	2.00
	133.06	C9H8O-H ⁺	e.g. Cinnamic acid	2.00		157.08	C8H12O3-H ⁺		2.00
	135.04	C8H6O2-H ⁺	e.g. Isophthalaldehyde, phenylglyoxal	2.00					
	135.08	C9H10O-H ⁺	e.g. 4-Ethylbenzaldehyde	2.00					
	137.06	C8H8O2-H ⁺	e.g. Benzeneacetic acid	2.00					
	141.05	C7H8O3-H ⁺		2.00					
	147.06	C9H6O2-H ⁺	e.g. Coumarin	2.00					
	149.02	C8H4O3-H ⁺	Phthalic anhydride	2.00					
	151.04	C8H6O3-H ⁺	e.g. Benzoylformic acid	2.00					
	151.08	C9H10O2-H ⁺	e.g. Hydrocinnamic acid	2.00					
	151.11	C10H14O-H ⁺	e.g. Verbenone	2.00					
	159.04	C10H6O2-H ⁺	Naphthalenedione	2.00					
	163.04	C9H6O3-H ⁺		2.00					
	169.07	C12H8O-H ⁺	e.g. dibenzofuran	2.00					
CHN									
	42.04	C2H3N-H ⁺	Acetonitrile	3.90		100.04	C4H5NO2-H ⁺		2.00
	54.04	C3H3N-H ⁺	Propenenitrile	2.00		112.05	C5H5NO2-H ⁺		2.00
	56.05	C3H5N-H ⁺	e.g. Propanenitrile	2.00		114.02	C4H3NO3-H ⁺	Nitrofuran	2.00
	68.05	C4H5N-H ⁺	e.g. Pyrrole	2.38		114.06	C5H7NO2-H ⁺	e.g. Ethyl cyanoacetate	2.00
	70.07	C4H7N-H ⁺	e.g. Butanenitrile	2.00		120.05	C7H5NO-H ⁺	e.g. Benzisoxazole	2.00
	84.09	C5H9N-H ⁺	e.g. Pentanenitrile	2.00		122.02	C2H3NO5-H ⁺	peroxyacetyl nitrate	2.00
	100.08	C5H9N3-H ⁺		2.00		122.07	C7H7NO-H ⁺	e.g. Benzamide	2.00
	104.05	C7H5N-H ⁺	Benzonitrile	2.00		124.05	C6H5NO2-H ⁺	Nitrobenzene	2.00
	118.06	C8H7N-H ⁺	Indole	2.00		136.04	C7H5NO2-H ⁺	e.g. 2-Furoylacetonitrile	2.00

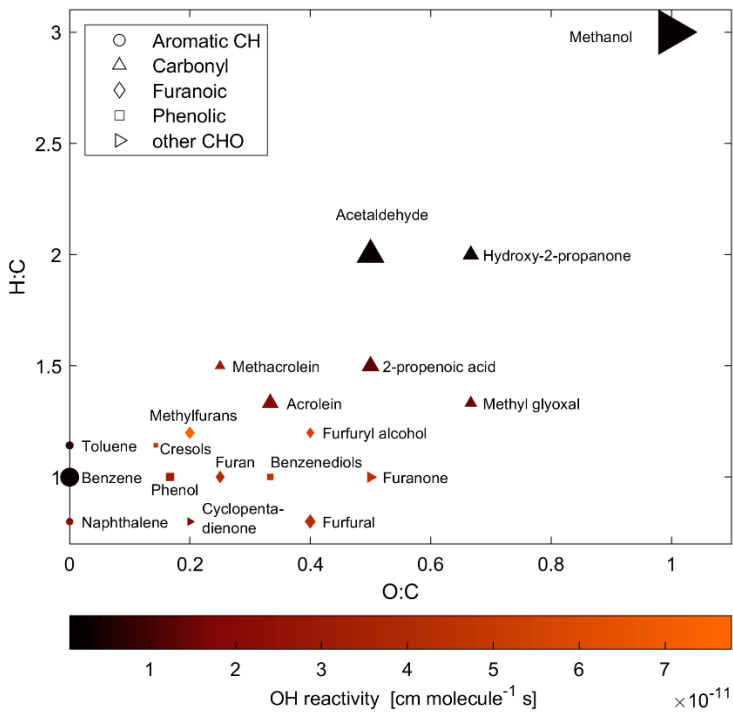


Figure S11: Van Krevelen diagram of selected VOCs commonly emitted from RWC. The marker size is scaled based on concentration in the fresh exhaust from spruce combustion in a modern masonry heater (Hartikainen et al., 2018), whereas the marker color indicates the compounds reactivity with OH.

105

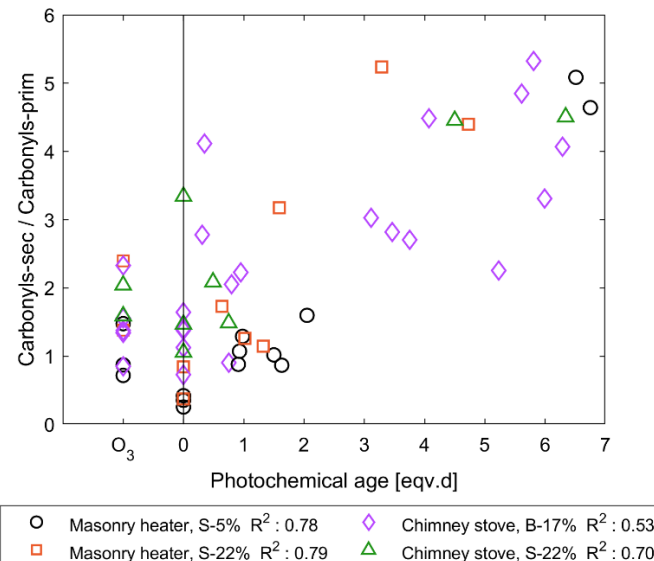


Figure S12: The ratios between the concentrations of the two carbonyl groups (secondary:primary) as the function of photochemical age.

110 **S4 Physical transformation of the particulate phase**

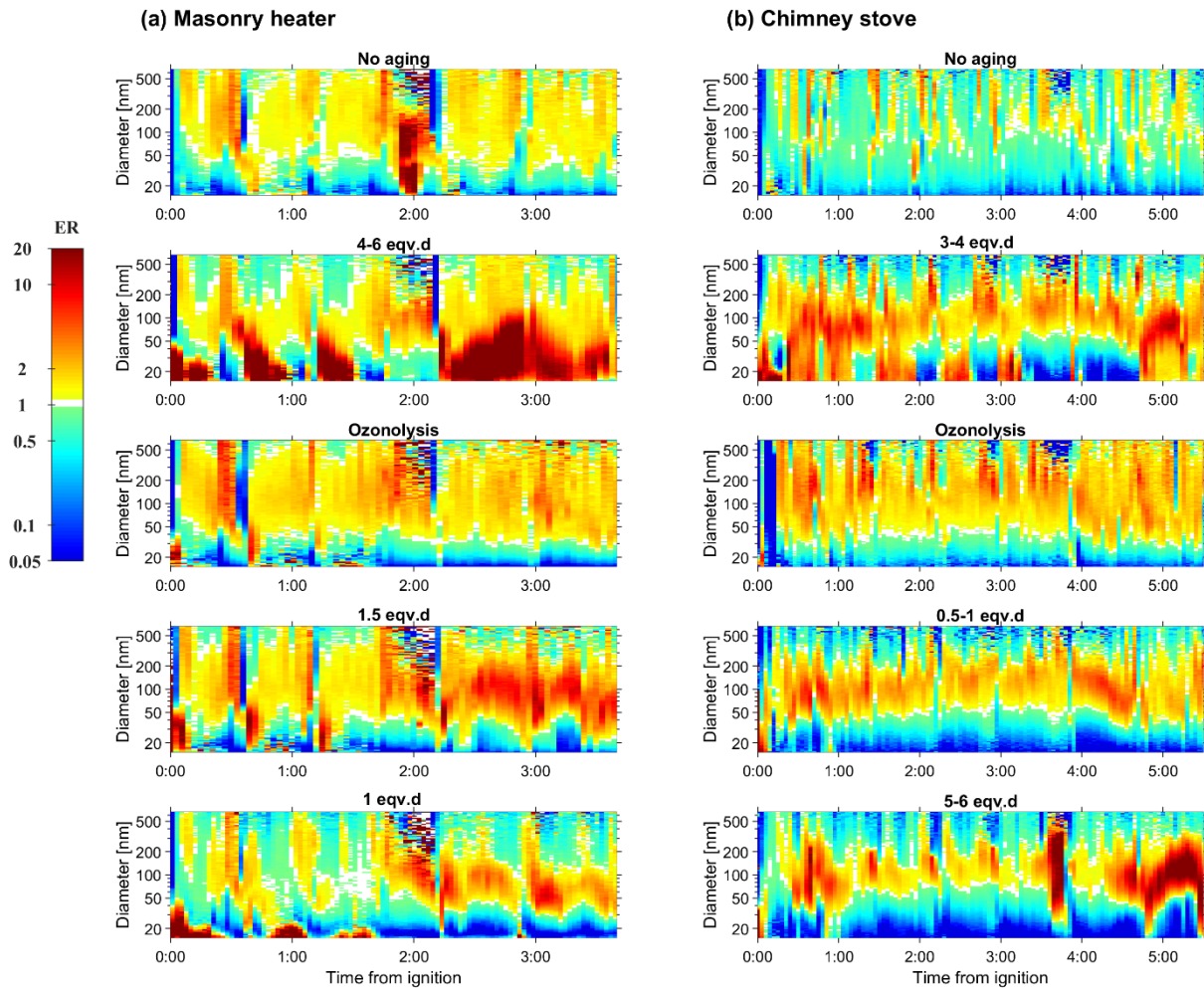
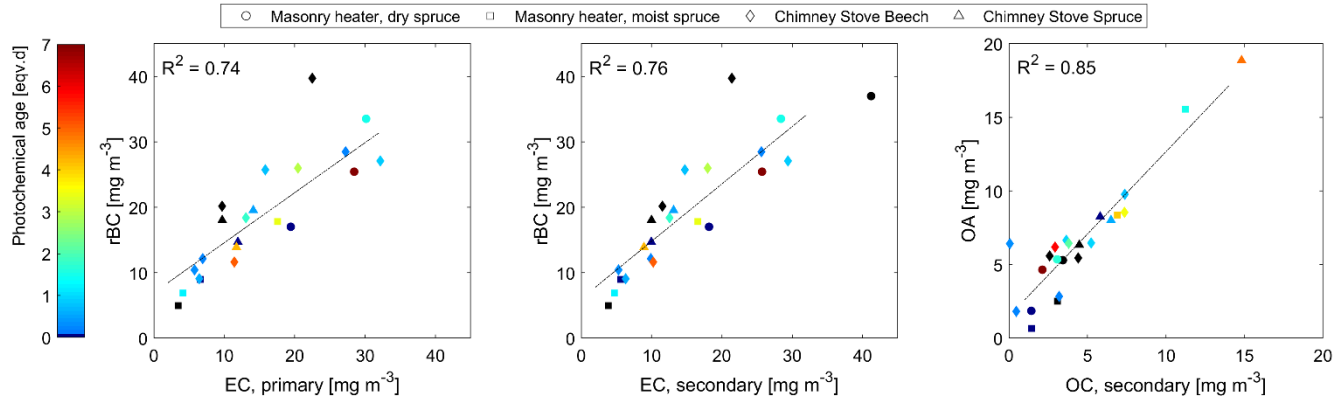


Figure S13: Particle number enhancement ratios (ER; secondary/primary) based on the SMPS measurements before and after PEAR.

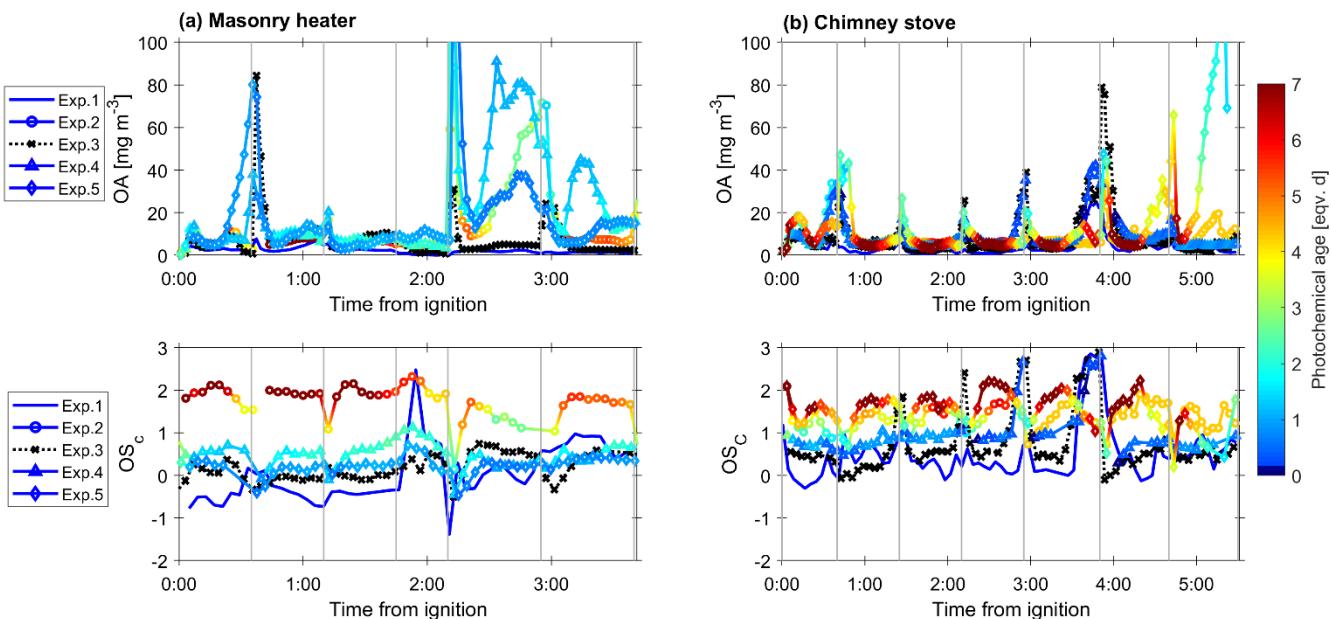
S5 Aerosol mass spectrometry analyses

115 The measurements of the non-refractory chemical species (Org, NO₃, SO₄, NH₄ and Chl) were conducted with the standard tungsten vaporizer, while the SP-AMS dual vaporizer mode was used to characterise the refractory black carbon (rBC) (Onasch et al., 2012). Standard mass-based calibrations were performed for the ionisation efficiency in the AMS using ammonium nitrate and Regal Black (Regal 400R Pigment Black, Cabot Corp.) particles (Jayne et al., 2000; Onasch et al., 2012). SP-AMS

was operated in V-mode from 12 to 555 m/z and the two vaporizer configurations were alternated every 120 s, including the
120 particle time-of-flight (PTOF) mode (duration 20 s). AMS data analysis was performed using the standard analysis tools SQUIRREL v1.62A and PIKA v1.22A adapted in Igor Pro 8 (Wavemetrics). The data was corrected for time-dependent background gas-phase CO₂ and for the interactions of inorganic salts with pre-deposited carbon on the tungsten vaporizer (Pieber et al., 2016) using a relative ionisation efficiency (RIE) of 1.4.



125 **Figure S14:** Correlations between variables measured by AMS after the PEAR and by thermal-optical analyses, respectively: (a) refractory black carbon (rBC) and elemental carbon (EC) before the PEAR; (b) rBC and EC after the PEAR; (c) organic aerosol (OA) and organic carbon (OC) after the PEAR.



130 **Figure S15:** Concentrations and average carbon oxidation states (OS_C) of particulate OA from (a) masonry heater and (b) chimney stove after PEAR in exhaust normalised to dry, 13 % O₂ flue gas. Black dotted lines indicate ozonolysis experiments.

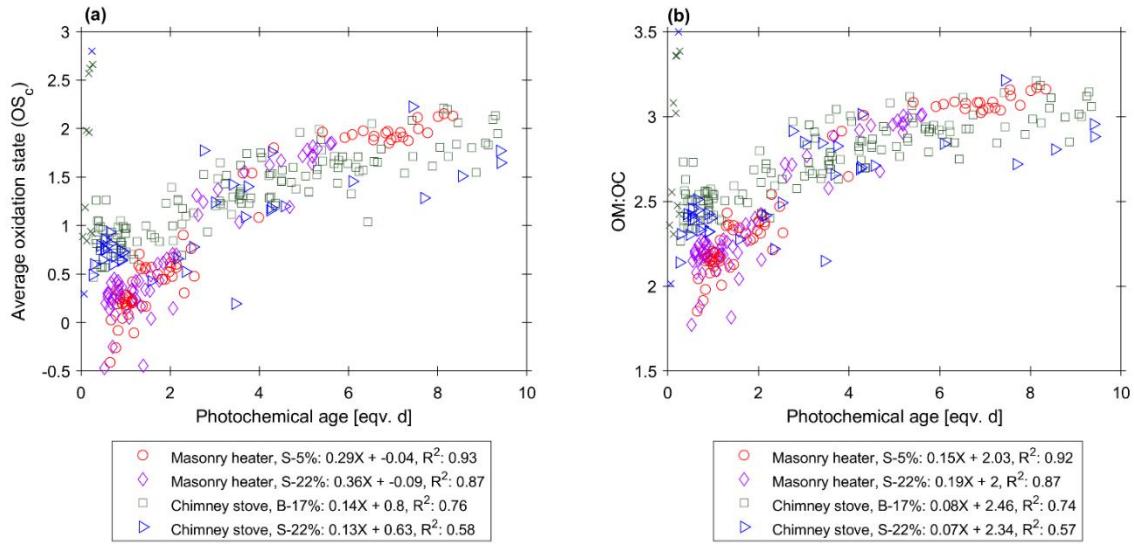


Figure 16: Relationship between photochemical age and (a) oxidation state and (b) OM:OC ratio during the photochemical aging experiments. Coefficients of determination (R^2) were calculated for the photochemical exposure range of 0.25-10 eqv.d. Values outside this age range (crossed over) were not considered.

Table S7: Average chemical composition of the OA (dilution corrected, dry, 13 % O₂) measured by AMS.

	Exp.	Fuel	Exposure [eqv.d]	O:C	H:C	OS _C	OM:OC	rBC mg m ⁻³	OA mg m ⁻³	PAH µg m ⁻³	NO ₃ mg m ⁻³	SO ₄ mg m ⁻³	NH ₄ mg m ⁻³	Chl mg m ⁻³
Masonry heater	1	S-5%		0.55	1.51	-0.18	1.86	28.89	3.10	98	0.16	0.17	0.00	0.17
		S-22%		0.82	1.33	0.15	2.20	21.77	1.57	27	0.11	0.13	0.00	0.12
	2	S-5%	6.72	1.45	1.06	0.92	3.02	42.83	7.63	16	1.92	0.80	0.79	0.02
		S-22%	4.02	1.30	1.12	0.64	2.83	48.03	24.98	80	1.50	1.08	0.96	0.03
	3	S-5%	O ₃	0.69	1.38	0.00	2.03	68.54	9.64	246	1.42	0.21	0.03	0.13
		S-22%	O ₃	0.81	1.28	0.15	2.19	12.15	6.61	180	0.84	0.25	0.03	0.06
	4	S-5%	0.94	0.90	1.31	0.22	2.31	59.40	9.58	105	1.27	0.44	0.16	0.04
		S-22%	0.73	0.84	1.33	0.17	2.23	17.70	44.11	485	1.00	0.38	0.49	0.04
	5	S-5%	1.71	0.76	1.36	0.07	2.13	47.08	13.69	241	1.36	0.27	0.16	0.05
		S-22%	1.46	0.78	1.34	0.11	2.16	24.47	24.54	455	1.20	0.37	0.24	0.03
Chimney stove	1	B-17%		0.86	1.25	0.22	2.26	23.03	3.86	65	0.34	1.08	0.00	0.28
		S-22%		1.47	0.91	0.41	2.32	27.97	4.02	80	0.21	1.13	0.00	0.31
	2	B-17%	3.61	1.25	1.14	0.63	2.76	21.60	8.78	23	5.07	1.66	1.38	0.02
		S-22%	~4	1.47	1.19	0.90	2.80	19.70	10.39	26	4.05	1.33	0.96	0.02
	3	B-17%	O ₃	1.01	1.15	0.41	2.44	26.24	8.33	114	3.32	1.82	0.22	0.12
		S-22%	O ₃	0.82	1.30	0.16	2.20	24.89	10.34	271	2.41	1.12	0.16	0.13
	4	B-17%	0.62	1.09	1.17	0.47	2.55	20.93	9.95	52	10.90	2.93	1.88	0.08
		S-22%	0.70	1.04	1.23	0.05	2.37	27.91	11.46	215	6.40	1.89	1.02	0.08
	5	B-17%	5.78	1.36	1.11	0.80	2.91	21.81	9.45	22	7.34	2.68	1.66	0.02
		S-22%	5.83	0.87	1.32	0.10	2.74	19.63	32.71	158	4.63	1.26	1.31	0.03

S5.1 Positive matrix factorisation analysis

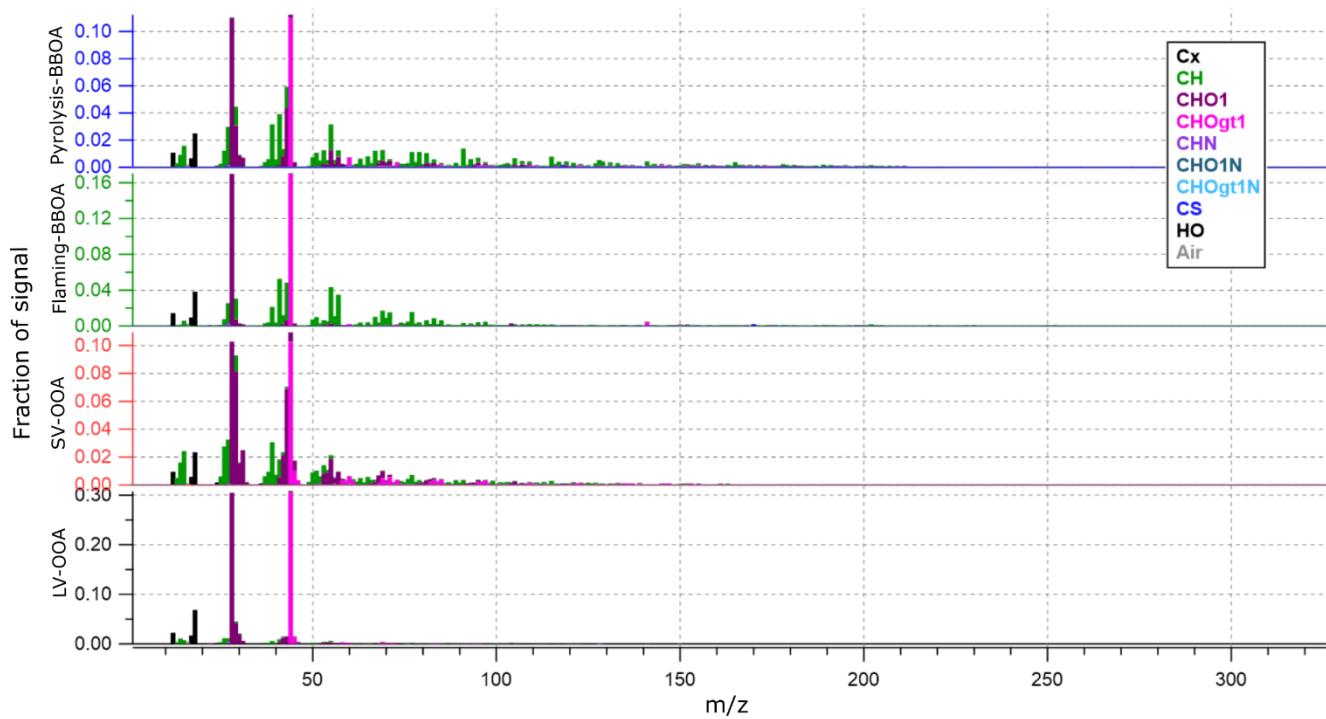


Figure S17: Spectra of the four factors identified from the AMS OA spectra by positive matrix factorisation analysis.

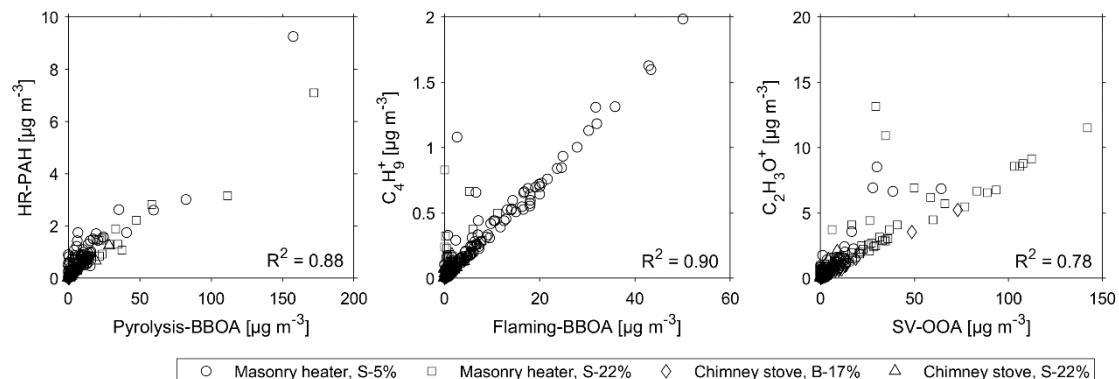


Figure S18: Correlations between (a) pyrolysis-BBOA and PAC concentration, (b) flaming-BBOA and C_4H_9^+ , and (c) SV-OOA to $\text{C}_2\text{H}_3\text{O}^+$.

S5.2 HR-PAH analysis

Table S8: Ions included in the HR-PAH analysis, based on the grouping by Herring et al. (2015). Analysis was adapted for RWC exhaust with an addition of polycyclic aromatic compounds typically released from RWC (Avagyan et al., 2016; Bertrand et al., 2018; Bruns et al., 2015; Czech et al., 2018; Miersch et al., 2019).

Unsubstituted PAHs (UnSubPAH)	Oxygenated PAHs (OPAH)	Methylated PAHs (MPAH)	Nitrogen-substituted PAHs (NPAH)	Amino PAHs (APAH)
C10H8	C9H8O	C11H10	C10H7NO2	C16H11N
C12H8	C11H8O	C12H12	C12H9NO2	C18H13NO
C12H10	C11H8O2*	C13H12	C13H9NO2	C20H13N
C13H10	C10H6O2	C14H12	C14H9NO2	C21H13N
C14H8	C12H8O	C15H12	C16H9NO2	
C14H10	C13H8O	C15H14	C13H8N2O4	
C15H10	C13H10O	C16H14	C18H11NO2	
C16H10	C12H6O3*	C17H16		
C17H12	C12H6O2	C18H14*		
C18H10	C12H8O2	C18H18		
C18H12	C12H8O3*	C19H14		
C20H10	C14H10O	C20H16		
C20H12	C13H8O2	C21H16		
C22H12	C15H8O			
C22H14	C14H8O2			
C24H12*	C15H8O2*			
	C16H8O2			
	C16H10O*			
	C17H10O*			
	C19H10O			
	C18H10O2			

* added for RWC

150 S6 In-situ derivatisation and thermal desorption - gas-chromatography - time-of-flight mass spectrometry

In-situ derivatisation and thermal desorption - gas-chromatography - time-of-flight mass spectrometry (IDTD-GC-ToFMS, (Orasche et al. 2011) was utilised in analysis of semi volatile organic target analytes in particulate phase. Subsamples were taken from the collected quartz fibre filters and prepared in GC-liners for the analyses. 10 µl Methyl-trimethylsilyl-trifluoroacetamid (MSTFA, Macherey-Nagel, Germany) was added automatically in each liner by the sampling robot (PAL

155 Focus, Atas GL, Netherlands) before samples were placed into a direct thermal desorption unit (Linex and Optic 3, Atas GL,

Netherlands). Furthermore, the samples were spiked with mixtures of isotope labelled internal standards and calibration standards for the purpose of calibration and quantification of the non-polar (Table S9) and polar (Table S10) compounds.

MSTFA was continuously added to the helium carrier gas on a 4 ml min⁻¹ stream, throughout the 16 minutes of thermal extraction at 300 °C. After the thermal extraction and derivatisation procedure, the pure helium flow was set back to 0.7 ml min⁻¹, with a split flow of 50 ml min⁻¹. IDTD was done at an isothermal GC temperature of 50° C in order to trap desorbed compounds at the front of the separation column before starting the GC-MS run. The column in use was an almost non-polar BPX5, 25 m, 0.22 mm ID, 0.25 µm film thicknesses (SGE, Australia), used in an Agilent 6890 gas chromatograph (Agilent, USA). Mass spectrometric detection in the range 35 to 500 m/z was carried out on a Pegasus III ToFMS (LECO, USA) using an acquisition frequency of 25 spectra per second. Evaluation of mass spectra was done with the ChromaTOF software package (LECO, USA).

Table S9: Isotope labelled internal standards for nonpolar compounds used in the IDTD-GC-ToFMS analyses.

Isotope labelled internal standard mixture	Calibration standard mixture
9,10-Anthracenedione 13C6	1(2H)-Acenaphthylenone
Acenaphthene d10	Benz[a]pyrene
Acenaphthylene d8	Benz[e]pyrene
Anthracene d10	Benzo[a]anthracene-7,12-dione
Benz[a]anthracene d12	Benzo[b]fluoranthene
Benz[a]pyrene d12	Benzo[b]fluoranthene
Benz[e]pyrene d12	Benzo[b]naphtho[1,2-d]thiophene
Benzo[a]anthracene-7,12-dione d10	Benzo[b]naphtho[2,1-d]furan
Benzo[b]fluoranthene d12	Benzo[b]naphtho[2,1-d]thiophene
Benzo[b]fluoranthene d12	Benzo[b]naphtho[2,3-d]furan
Benzo[ghi]perylene d12	Benzo[c]phenanthrene
Benzo[k]fluoranthene d12	Benzo[ghi]perylene
Benzo[k]fluoranthene d12	Benzo[k]fluoranthene
Biphenyl d10	Benzo[k]fluoranthene
Chrysene d12	Biphenyl
Coronene d12	Chrysene
Dibenz[ah]anthracene d14	Coronene
Dibenzothiophene d8	Cyclopenta(def)phenanthrenone
Docosane d46	Dibenz[ac]anthracene
Eicosane d42	Dibenz[ah]anthracene
Fluoranthene d10	Dibenzothiophene
Fluorene d10	Fluoranthene
Hexadecane d34	Fluorene
Indeno[1,2,3-cd]pyrene d12	Indeno[1,2,3-cd]pyrene
Naphthalene d8	Methyleicosanoate
Octadecane d38	n-Alkanes C12-C40
Perylene d12	Naphthalene
Phenanthrene d10	Naphtho[2,1,8,7-klmn]xanthene
Pyrene d10	Perylene
Tetracosane d50	Phenanthrene
Triacontane d62	Picene
	Pyrene
	Retene
	Xanthone

Table S10: Isotope labelled internal standards used for polar compounds in the IDTD-GC-ToFMS analyses.

Isotope labelled internal standard mixture	Calibration standard mixture
4-Nitrophenol d4	1-Hydroxypyrene
Adipic acid d10	2-Hydroxy-1-naphthaldehyde
Cholesterol d6	2-Ketoglutaric acid
Dodecanol d25	2-Methyl-4-Nitrophenol
Fumaric acid d2	2-Methylerythritol
Glucose 13C6	2-Naphthalanol
Glycerol d8	3-Hydroglutaric acid
Levoglucosan 13C6	3-Hydroxyphenanthrene
Palmitic acid d31	4-Hydroxyphenanthrene
Vanillin 13C6	4-Nitrocatechol
	4-Nitrophenol
	9-Hydroxyphenanthrene
	Abietic acid
	Acetosyringone
	Adipic Acid
	Azelaic acid
	Butanedioic acid
	Cholesterol
	Coniferaldehyde
	Ergosterol
	Erythritol
	Fumaric acid
	Galactosan
	Glutaric acid
	Hexanedioic acid
	Hexanoic acid
	Isopimaric acid
	Levoglucosan
	Linoleic acid
	Maleic acid
	Malic acid
	Malonic acid
	Mannosan
	Methyl vanillate
	Oleic acid
	Palmitic acid
	Phthalic acid
	Salicylic acid
	Sorbit
	Stearic acid
	Syringic Acid
	Tartaric acid
	Threitol
	Trimellitic acid
	Vanillic acid
	Vanillin

170

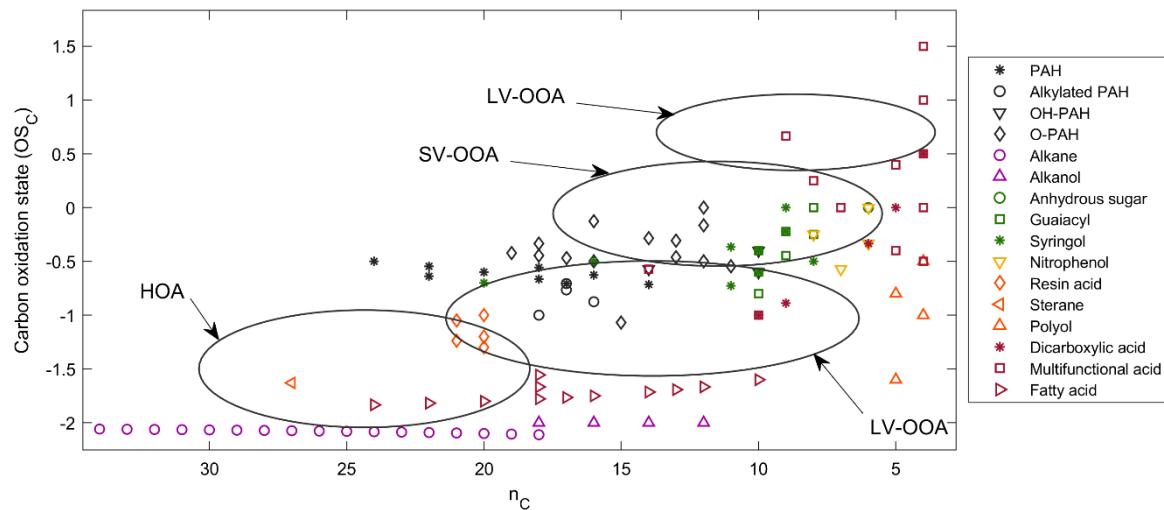


Figure S19: Compounds analysed by IDTD-GC-ToFMS displayed in the OS_C - n_C space. The ambient organic aerosol classes identified by Kroll et al. (2011) are presented as an approximate reference for average hydrocarbon-like OA (HOA), primary biomass burning OA (BBOA), semi-volatile oxidised OA (SV-OOA) and low-volatility oxidised OA (LV-OOA).

175

Table S11: Pearson correlation coefficients between the particulate organic aerosol constituents measured by AMS (PMF and HR-PAH) and IDTD-GC-TOF-MS.

		PMF factors				HR-PAH					
		Pyrolysis-BBOA	Flaming-BBOA	SV-OOA	LV-OOA	Total	Unsub-PAH	OPAH	MPAH	NPAH	APAH
PMF factors	Pyrolysis-BBOA	1.00	0.17	0.40	-0.02	0.96	0.96	0.87	0.97	0.86	0.89
	Flaming-BBOA	0.17	1.00	-0.07	-0.21	0.19	0.21	0.17	0.14	0.17	0.21
	SV-OOA	0.40	-0.07	1.00	0.35	0.48	0.44	0.70	0.38	0.68	0.57
	LV-OOA	-0.02	-0.21	0.35	1.00	-0.02	-0.04	0.09	-0.04	0.06	0.03
HR-PAH	Total	0.96	0.19	0.48	-0.02	1.00	1.00	0.94	0.99	0.94	0.96
	UnsubPAH	0.96	0.21	0.44	-0.04	1.00	1.00	0.93	0.99	0.93	0.95
	OPAH	0.87	0.17	0.70	0.09	0.94	0.93	1.00	0.88	0.98	0.94
	MPAH	0.97	0.14	0.38	-0.04	0.99	0.99	0.88	1.00	0.88	0.92
	NPAH	0.86	0.17	0.68	0.06	0.94	0.93	0.98	0.88	1.00	0.97
	APAH	0.89	0.21	0.57	0.03	0.96	0.95	0.94	0.92	0.97	1.00
IDTD-GC-ToF-MS	PAH	0.01	0.64	-0.22	-0.17	0.19	0.27	0.04	0.15	0.09	0.09
	OH-PAHs	0.31	-0.05	0.88	0.65	0.75	0.65	0.92	0.54	0.88	0.87
	Carbonyl-PAHs	0.50	-0.12	0.49	0.35	0.69	0.67	0.74	0.52	0.65	0.58
	alkylated PAHs	0.01	0.75	-0.16	-0.26	0.21	0.29	0.01	0.24	0.09	0.14
	alkanes	-0.10	0.31	-0.19	-0.38	-0.17	-0.12	-0.25	-0.10	-0.22	-0.17
	alkanols	-0.11	0.26	0.43	0.70	0.22	0.17	0.36	0.06	0.35	0.38
	anhydrous sugars	0.53	-0.24	0.70	0.35	0.68	0.61	0.71	0.65	0.78	0.76
	guaiacyls	0.10	0.26	0.10	-0.09	0.29	0.30	0.21	0.26	0.28	0.28
	nitro phenols	-0.17	-0.14	0.60	0.76	0.09	-0.03	0.37	-0.08	0.32	0.31
	resin acids	0.63	0.23	-0.24	-0.42	0.45	0.54	0.09	0.66	0.25	0.24
	polyols	0.27	-0.09	0.93	0.63	0.71	0.61	0.89	0.51	0.87	0.87
	dicarboxylic acids	0.12	-0.01	0.87	0.74	0.63	0.53	0.83	0.40	0.80	0.81
	multifunctional acids/ anhydrides	-0.10	-0.16	0.93	0.89	0.40	0.26	0.71	0.15	0.66	0.67
	fatty acids	-0.05	0.50	-0.40	-0.34	-0.08	0.01	-0.26	-0.01	-0.21	-0.15

Table S12: Secondary concentrations (ng m⁻³) of compounds measured by IDTD-GC-ToFMS. Normalised to dry, 13 % O₂ flue gas conditions. Attached as a .xlsx file.

References

- Atkinson, R., Baulch, D. L., Cox, R. A., Crowley, J. N., Hampson Jr, R. F., Kerr, J. A., Rossi, M. J. and Troe, J.: Summary of evaluated kinetic and photochemical data for atmospheric chemistry, IUPAC Subcommittee on gas kinetic data evaluation for atmospheric chemistry, 20, 2001.
- 185 Atkinson, R.: Kinetics and mechanisms of the gas-phase reactions of the hydroxyl radical with organic compounds under atmospheric conditions, *Chem. Rev.*, 86, 69-201, 1986.
- Atkinson, R., Aschmann, S. M. and Carter, W. P.: Kinetics of the reactions of O₃ and OH radicals with furan and thiophene at 298±2 K, *Int J Chem Kinet*, 15, 51-61, 1983.
- Avagyan, R., Nyström, R., Lindgren, R., Boman, C. and Westerholm, R.: Particulate hydroxy-PAH emissions from a 190 residential wood log stove using different fuels and burning conditions, *Atmos. Environ.*, 140, 1-9, 2016.
- Barmet, P., Dommen, J., DeCarlo, P. F., Tritscher, T., Praplan, A. P., Platt, S. M., Prvt, A., Donahue, N. M. and Baltensperger, U.: OH clock determination by proton transfer reaction mass spectrometry at an environmental chamber, *Atmos. Meas. Tech.*, 5, 647, 2012.
- Baulch, D. L., Cobos, C. J., Cox, R. A., Frank, P., Hayman, G., Just, T., Kerr, J. A., Murrells, T., Pilling, M. J., Troe, J., 195 Walker, W. and Warnatz, J.: Evaluated kinetic data for combustion modeling. Supplement I, *J. Phys. Chem. Ref. Data*, 23, 847-848, 1994.
- Baulch, D. L., Cobos, C., Cox, R. A., Esser, C., Frank, P., Just, T., Kerr, J. A., Pilling, M. J., Troe, J. and Walker, R. W., and Warnatz, J.: Evaluated kinetic data for combustion modelling, *J. Phys. Chem. Ref. Data*, 21, 411-734, 1992.
- Bertrand, A., Stefenelli, G., Jen, C. N., Pieber, S. M., Bruns, E. A., Ni, H., Temime-Roussel, B., Slowik, J. G., Goldstein, A. 200 H., El Haddad, I., Baltensperger, U., Prévôt, A. S. H., Wortham, H. and Marchand, N.: Evolution of the chemical fingerprint of biomass burning organic aerosol during aging, *Atmos. Chem. Phys.*, 18, 7607-7624, 2018.
- Bruns, E. A., Krapf, M., Orasche, J., Huang, Y., Zimmermann, R., Drinovec, L., Močnik, G., El-Haddad, I., Slowik, J. G., Dommen, J., Baltensperger, U. and Prévôt, A S H: Characterization of primary and secondary wood combustion products generated under different burner loads, *Atmos. Chem. Phys.*, 15, 2825-2841, 2015.
- 205 Cappellin, L., Karl, T., Probst, M., Ismailova, O., Winkler, P. M., Soukoulis, C., Aprea, E., Märk, T. D., Gasperi, F. and Biasioli, F.: On quantitative determination of volatile organic compound concentrations using proton transfer reaction time-of-flight mass spectrometry, *Environ. Sci. Technol.*, 46, 2283-2290, 2012.
- Cvetanović, R. J.: Evaluated chemical kinetic data for the reactions of atomic oxygen O (3P) with unsaturated hydrocarbons, *J. Phys. Chem. Ref. Data*, 16, 261-326, 1987.

- 210 Czech, H., Miersch, T., Orasche, J., Abbaszade, G., Sippula, O., Tissari, J., Michalke, B., Schnelle-Kreis, J., Streibel, T., Jokiniemi, J. and Zimmermann, R.: Chemical composition and speciation of particulate organic matter from modern residential small-scale wood combustion appliances, *Sci. Total Environ.*, 612, 636-648, 2018.
- Grosjean, E. and Grosjean, D.: Rate constants for the gas-phase reaction of ozone with 1, 1-disubstituted alkenes, *Int J Chem Kinet*, 28, 911-918, 1996.
- 215 Hartikainen, A., Yli-Pirilä, P., Tiitta, P., Leskinen, A., Kortelainen, M., Orasche, J., Schnelle-Kreis, J., Lehtinen, K. E., Zimmermann, R., Jokiniemi, J. and Sippula O.: Volatile organic compounds from logwood combustion: emissions and transformation under dark and photochemical aging conditions in a smog chamber, *Environ. Sci. Technol.*, 52, 4979-4988, 2018.
- Herron, J. T.: Evaluated chemical kinetic data for the reactions of atomic oxygen O (3P) with saturated organic compounds in
220 the gas phase, *J. Phys. Chem. Ref. Data*, 17, 967-1026, 1988.
- Herring, C. L., Faiola, C. L., Massoli, P., Sueper, D., Erickson, M. H., McDonald, J. D., Simpson, C. D., Yost, M. G., Jobson, B. T. and VanReken, T. M.: New methodology for quantifying polycyclic aromatic hydrocarbons (PAHs) using high-resolution aerosol mass spectrometry, *Aerosol Sci. Tech.*, 49, 1131-1148, 2015.
- Jayne, J. T., Leard, D. C., Zhang, X., Davidovits, P., Smith, K. A., Kolb, C. E. and Worsnop, D. R.: Development of an aerosol
225 mass spectrometer for size and composition analysis of submicron particles, *Aerosol. Sci. Technol.*, 33, 49-70, 2000.
- Keller-Rudek, H., Moortgat, G. K., Sander, R. and Sørensen, R.: The MPI-Mainz UV/VIS Spectral Atlas of Gaseous Molecules of Atmospheric Interest, [online] Available from: www.uv-vis-spectral-atlas-mainz.org, 2015.
- Kroll, J. H., Donahue, N. M., Jimenez, J. L., Kessler, S. H., Canagaratna, M. R., Wilson, K. R., Altieri, K. E., Mazzoleni, L. R., Wozniak, A. S., Bluhm, H., Mysak, E. R., Smith, J. D., Kolb, C. E. and Worsnop, D. R.: Carbon oxidation state as a metric
230 for describing the chemistry of atmospheric organic aerosol, *Nat. Chem.*, 3, 133, 2011.
- Lehtinen, K. E., Korhonen, H., Maso, M. D. and Kulmala, M.: On the concept of condensation sink diameter, *Boreal Environ. Res.*, 8, 405-412, 2003.
- Miersch, T., Czech, H., Hartikainen, A., Ihlainen, M., Orasche, J., Abbaszade, G., Tissari, J., Streibel, T., Jokiniemi, J., Sippula, O. and Zimmermann, R.: Impact of photochemical ageing on Polycyclic Aromatic Hydrocarbons (PAH) and
235 oxygenated PAH (Oxy-PAH/OH-PAH) in logwood stove emissions, *Sci. Total Environ.*, 686, 382-392, 2019.
- Onasch, T. B., Trimborn, A., Fortner, E. C., Jayne, J. T., Kok, G. L., Williams, L. R., Davidovits, P. and Worsnop, D. R.: Soot Particle Aerosol Mass Spectrometer: Development, Validation, and Initial Application, *Aerosol Sci. Tech.*, 46, 804-817, 2012.
- Orasche, J., Schnelle-Kreis, J., Abbaszade, G. and Zimmermann, R.: In-situ derivatization thermal desorption GC-TOFMS for direct analysis of particle-bound non-polar and polar organic species, *Atmos. Chem. Phys.*, 11, 8977-8993, 2011.

- 240 Palm, B. B., Campuzano-Jost, P., Ortega, A. M., Day, D. A., Kaser, L., Jud, W., Karl, T., Hansel, A., Hunter, J. F., Cross, E. S., Kroll, J. H., Peng, Z., Brune, W. H. and Jimenez, J. L.: In situ secondary organic aerosol formation from ambient pine forest air using an oxidation flow reactor, *Atmos. Chem. Phys.*, 16, 2943-2970, 2016.
- Paulson, S. E., Orlando, J. J., Tyndall, G. S. and Calvert, J. G.: Rate coefficients for the reactions of O (3P) with selected biogenic Hydrocarbons, *Int J Chem Kinet*, 27, 997-1008, 1995.
- 245 Peng, Z., Day, D. A., Ortega, A. M., Palm, B. B., Hu, W., Stark, H., Li, R., Tsigaridis, K., Brune, W. H. and Jimenez, J. L.: Non-OH chemistry in oxidation flow reactors for the study of atmospheric chemistry systematically examined by modeling, *Atmos. Chem. Phys.*, 16, 4283-4305, 2016.
- Peng, Z. and Jimenez, J. L.: Modeling of the chemistry in oxidation flow reactors with high initial NO, *Atmos. Chem. Phys.*, 17, 11991-12010, 2017.
- 250 Pieber, S. M., El Haddad, I., Slowik, J. G., Canagaratna, M. R., Jayne, J. T., Platt, S. M., Bozzetti, C., Daellenbach, K. R., Fröhlich, R., Vlachou, A., Klein F., Dommen, J., Miljevic, B., Jiménez J. L., Worsnop D. R., Baltensperger, U. and Prévôt A. S. H.: Inorganic salt interference on CO₂ in aerodyne AMS and ACSM organic aerosol composition studies, *Environ. Sci. Technol.*, 50, 10494-10503, 2016.
- Stedman, D. H. and Niki, H.: Ozonolysis rates of some atmospheric gases, *Environ. Lett.*, 4, 303-310, 1973.
- 255 Tang, M. J., Shiraiwa, M., Pöschl, U., Cox, R. A. and Kalberer, M.: Compilation and evaluation of gas phase diffusion coefficients of reactive trace gases in the atmosphere: Volume 2. Diffusivities of organic compounds, pressure-normalised mean free paths, and average Knudsen numbers for gas uptake calculations, *Atmos. Chem. Phys.*, 15, 5585-5598, 2015.
- Toby, S., Van de Burgt, L J and Toby, F. S.: Kinetics and chemiluminescence of ozone-aromatic reactions in the gas phase, *J. Phys. Chem.*, 89, 1982-1986, 1985.